



HAL
open science

Electron-impact excitation of diatomic hydride cations - I. HeH⁺, CH⁺, ArH⁺

James R. Hamilton, Alexandre Faure, Jonathan Tennyson

► **To cite this version:**

James R. Hamilton, Alexandre Faure, Jonathan Tennyson. Electron-impact excitation of diatomic hydride cations - I. HeH⁺, CH⁺, ArH⁺. Monthly Notices of the Royal Astronomical Society, 2016, 455, pp.3281-3287. 10.1093/mnras/stv2429 . insu-03691576

HAL Id: insu-03691576

<https://hal-insu.archives-ouvertes.fr/insu-03691576>

Submitted on 9 Jun 2022

HAL is a multi-disciplinary open access archive for the deposit and dissemination of scientific research documents, whether they are published or not. The documents may come from teaching and research institutions in France or abroad, or from public or private research centers.

L'archive ouverte pluridisciplinaire **HAL**, est destinée au dépôt et à la diffusion de documents scientifiques de niveau recherche, publiés ou non, émanant des établissements d'enseignement et de recherche français ou étrangers, des laboratoires publics ou privés.

Electron-impact excitation of diatomic hydride cations – I. HeH^+ , CH^+ , ArH^+

James R. Hamilton,¹ Alexandre Faure² and Jonathan Tennyson¹★

¹Department of Physics and Astronomy, University College, London, Gower St., London WC1E 6BT, UK

²UJF-Grenoble 1 / CNRS-INSU, Institut de Planétologie et d'Astrophysique de Grenoble (IPAG) UMR 5274, Grenoble F-38041, France

Accepted 2015 October 19. Received 2015 October 1; in original form 2015 July 17

ABSTRACT

R-matrix calculations combined with the adiabatic nuclei approximation are used to compute electron-impact rotational excitation rates for three closed-shell diatomic cations, HeH^+ , CH^+ , ArH^+ . Comparisons with previous studies show that an improved treatment of threshold effects leads to significant changes in the low temperature rates; furthermore the new calculations suggest that excitation of CH^+ is dominated by $\Delta J = 1$ transitions as is expected for cations with a large dipole moment. A model for ArH^+ excitation in the Crab nebula is presented which gives results consistent with the observations for electron densities in the range $2\text{--}3 \times 10^3 \text{ cm}^{-3}$.

Key words: molecular processes – ISM: molecules.

1 INTRODUCTION

Because hydrogen is much more abundant than any other element in the interstellar medium (ISM), hydrides are the first molecules to form. They therefore constitute significant reservoirs of heavy elements, as well as sensitive tests of interstellar chemistry networks and of the ambient physical conditions. Hydrides are also employed to trace specific aspects of interstellar environments. For example, in diffuse interstellar clouds, hydroxyl and water cations, OH^+ and H_2O^+ , are useful probes of the cosmic ray ionization rate (Indriolo et al. 2012), which controls the abundance of several interstellar molecules. Hydrogen fluoride, HF, is formed by the direct reaction of H_2 with F and can be employed as a proxy for molecular hydrogen, see Indriolo et al. (2013) and references therein. The methylidyne and mercapto cations, CH^+ and SH^+ , are good tracers of warm regions, heated by shocks or the dissipation of turbulence, where endothermic reactions can occur, e.g. Godard et al. (2012). The argonium cation, ArH^+ , was the first noble gas molecular ion detected in space (Barlow et al. 2013) and it has been shown to be a tracer of almost purely atomic gas in the diffuse ISM (Schilke et al. 2014). As discussed by Jimenez-Redondo et al. (2014), molecular ions, such as ArH^+ , are also important constituents of cold terrestrial plasmas.

In diffuse clouds, hydrides can be observed through optical/ultraviolet absorption lines superposed on the spectra of background stars. At longer wavelengths, rotational transitions of hydrides can be observed in both absorption and emission, providing a large sampling of molecular regions, e.g. Gerin et al. (2010). In contrast to absorption line studies, which provide simple and reli-

able estimates of column densities, the interpretation of emission lines is much more problematic. The density of the dominant colliders (H, He, H_2 and electrons) is indeed often close to the critical density.¹ In such conditions, deviations from local-thermodynamic equilibrium (LTE) are expected and detailed radiative transfer modelling is necessary to derive both the physical conditions (density and temperature) and the column densities. Radiative transfer calculations in turn require a good knowledge of rate coefficients for collisional excitation. Despite recent experimental progress, these coefficients are difficult to measure and theory is needed to provide comprehensive sets of collisional data.

Significant progress was made in recent years in computing collisional rates for interstellar molecules, see Roueff & Lique (2013) for a review on collisions with H, He and H_2 . In regions where the electron fraction, n_e/n_H , is larger than $\sim 10^{-5}\text{--}10^{-4}$, electron-impact excitation can compete or even dominate over the neutrals (H, He and H_2). For example, in the photon-dominated region (PDR) associated with the Orion bar, van der Tak et al. (2012) have shown that the excitation of HF is driven by electron collisions with densities $n_e \sim 10 \text{ cm}^{-3}$. A similar result was obtained recently for OH^+ emission (van der Tak et al. 2013; Gómez-Carrasco et al. 2014). Electron-impact excitation of diatomic hydride cations thus appears as a crucial process in the ionized regions of the molecular ISM.

To date, five diatomic hydride cations have been detected in the ISM: CH^+ (Douglas & Herzberg 1941), OH^+ (Wyrowski et al. 2010), SH^+ (Menten et al. 2011), HCl^+ (De Luca et al. 2012) and very recently ArH^+ (Barlow et al. 2013). Thus far searches for

¹ The critical density defines, for a given transition or level, the density at which the spontaneous radiative rate equals the collisional rate.

★E-mail: j.tennyson@ucl.ac.uk

HeH⁺ have not been successful (Moorhead et al. 1988; Liu et al. 1997; Zinchenko, Dubrovich & Henkel 2011), except for a tentative detection in the remnant of supernova 1987A (Miller et al. 1992). We note that HeH⁺ is thought to be the first molecular species to appear in the Universe (Lepp, Stancil & Dalgarno 2002).

At ISM temperatures, the process of electron impact rotational excitation of hydrides should have a clearly observable effect. However, the process of dissociative recombination competes with excitation; results presented later in this work show that the cross-section for the rotational excitation of CH⁺ in the dominant channel $J = 0$ to $J = 1$ is 10–100 times higher than the summed experimental dissociative recombination cross-section of CH⁺ at the same temperature (Amitay & Zajfman 1996). The cross-section for rotational excitation for the same channel of HeH⁺ is also found to be similarly greater than the summed theoretical dissociative recombination cross-sections computed by Sarpal, Tennyson & Morgan (1994), albeit not at resonance regions in the dissociative recombination cross-section which nonetheless never exceeded the magnitude of the rotational excitation cross-section.

In this work, electron-impact rotational-excitation rate coefficients are calculated for HeH⁺, CH⁺ and ArH⁺, which all have a ground electronic state of symmetry $^1\Sigma^+$. The **R**-matrix method is combined with the adiabatic-nuclei-rotation (ANR) approximation to obtain rotational cross-sections at electron energies below 5 eV. It should be noted that previous **R**-matrix studies on HeH⁺ (Rabadán, Sarpal & Tennyson 1998) and CH⁺ (Lim, Rabadán & Tennyson 1999) were carried out but, particularly for the CH⁺ problem, the accuracy was compromised by the use of reduced treatments of polarization and a small close-coupling expansions. In both cases, the use of an improper threshold correction made the results less accurate at low electron temperatures. These limitations are overcome in the present work, as detailed below. In Section 2, the **R**-matrix calculations are described and the procedure used to derive the cross-sections is briefly introduced. In Section 3, we present and discuss the calculated rate coefficients. A model for the excitation of ArH⁺ in the Crab nebula is also presented in Section 4. Conclusions are summarized in Section 5.

2 CALCULATIONS

2.1 R-matrix calculations

In this paper, we present results for the electron collision calculations with molecular ions ArH⁺, HeH⁺ and CH⁺. These calculations employ the polyatomic **R**-matrix method and are adapted to calculate the rotational excitation cross-sections for specific transitions of the angular momentum quantum number, J , of the molecules. The **R**-matrix method is a sophisticated way of performing electron scattering calculations. For a full derivation of the **R**-matrix method and its application in electron scattering see Tennyson (2010). Here we used the Quantemol-N expert system (Tennyson et al. 2007) to run the UK molecular **R**-matrix codes (UKRMol Carr et al. 2012).

The calculations for all three molecules used **R**-matrix radii of 13 a_0 and Gaussian Type Orbitals (GTOs) to represent both the target and the continuum. Continuum orbitals up to g -wave ($\ell \leq 4$) were explicitly included in the calculations. The initial calculations for molecules were carried out using C_{2v} symmetry. In order to calculate the rotational excitation cross-sections of the molecules, however, the **T**-matrices were transformed into the $C_{\infty v}$ point group, the natural point group of the diatomic molecules.

The transformed **T**-matrices formed the input to electron-impact rotational excitation code ROTIONS (Rabadán & Tennyson 1998).

The technical details of the calculations are described below.

2.1.1 ArH⁺

The ArH⁺ target was represented using an augmented aug-cc-pVTZ GTO basis set. The use of augmented basis sets improves the treatment of the more diffuse orbitals of the excited states in the calculation. The quantum chemistry program MOLPRO (Werner et al. 2010) was used to do initial Hartree–Fock calculations on the ArH⁺ ground state using an aug-cc-pVTZ basis set. These ground state orbitals were then used in the **R**-matrix calculation. The target was represented using complete active space configuration interaction (CAS-CI) treatment involving freezing 10 electrons in $1\sigma^2 2\sigma^2 3\sigma^2 1\pi^4$ orbitals and distributing the remaining 8 electrons in the orbitals: $[4\sigma 5\sigma 2\pi 6\sigma 7\sigma 8\sigma 3\pi 9\sigma]^8$. Five states per symmetry generated from the initial CAS-CI calculation were used in the final close-coupling calculation with an excitation energy cut-off of 30 eV. This helps to converge the polarization effects introduced by the coupling to excited states of the molecule.

In the Earth’s atmosphere the isotope of argon in overwhelming abundance is ⁴⁰Ar (exact mass 39.962 38 u) as this isotope is created by the decay of ⁴⁰K. However, astronomically the major isotope of argon is ³⁶Ar (exact mass 35.967 55 u). A third stable isotope of argon is known to exist in nature, ³⁸Ar (exact mass 37.9627 u). ³⁸Ar is the least abundant natural isotope and is not significant terrestrially or astronomically. The dipole moment is important when calculating rotational excitation cross-sections and, for ionic molecules, the dipole moment depends upon the molecular centre of mass. This means that the dipole differs between isotopologues.

Our calculated dipole moment for ³⁶ArH⁺ is $\mu = 2.1425$ D, for ³⁸ArH⁺ $\mu = 2.1517$ D and for ⁴⁰ArH⁺ $\mu = 2.1595$ D, with rotational constant $B = 10.27$ cm⁻¹ for all three. The best available theoretical value for ⁴⁰ArH⁺ at its equilibrium geometry is $\mu = 2.177$ D (Cheng et al. 2007). By applying the same ratio to this latter value as was found with our calculations, our best estimates are $\mu = 2.169$ D for ³⁸ArH⁺ and $\mu = 2.160$ D for ³⁶ArH⁺. The experimental value for the rotational constant of ³⁶ArH⁺, from the Cologne Database for Molecular Spectroscopy (CDMS), is $B = 10.30$ cm⁻¹ (Müller et al. 2005) and this is taken to be the value for ³⁸ArH⁺ and ⁴⁰ArH⁺ also. We note that the rotational constants for the three isotopologues actually differ by 0.01 cm⁻¹ but this effect, as well as corrections due to centrifugal distortion, can be ignored in our treatment as they only influence the threshold correction we employ (see below) and this assumption itself introduces much larger uncertainties at low temperature. On the other hand, the small change in dipole values was taken into account since the Coulomb–Born correction scales with the square of the dipole.

2.1.2 HeH⁺

The HeH⁺ target was represented using a cc-pVTZ GTO basis set. Augmented basis sets gave result which showed artificial structure as function of electron collision energy. This is a signature of problems with linear dependence and probably caused by an excessive overlap between the augmented functions and the molecule continuum functions. The ground state electron occupation of HeH⁺ is $1\sigma^2$. As HeH⁺ is a two-electron system both its target wavefunction and the scattering wavefunction were represented with a full CI treatment, i.e. by allowing the electrons to freely occupy all

orbitals. All generated states up to 42 eV were retained in the final close-coupling calculation.

Our calculated HeH⁺ equilibrium geometry dipole moment and rotational constant are $\mu = 1.7168$ D and $B = 35.241$ cm⁻¹. The best available theoretical value for the dipole is $\mu = 1.664$ D (Pavanello et al. 2005) while the CDMS rotational constant is $B = 33.559$ cm⁻¹ (Müller et al. 2005).

2.1.3 CH⁺

The CH⁺ target was represented using a cc-pVTZ GTO basis set. Again, augmented basis sets did not give smooth results. The ground state of CH⁺ has the configuration $[1\sigma\ 2\sigma\ 3\sigma]^6$. The target was represented using CAS-CI treatment freezing the lowest energy $2\sigma^2$ orbital and placing the highest 4 electrons in orbitals $[2\sigma\ 3\sigma\ 1\pi\ 4\sigma\ 5\sigma\ 2\pi]^4$. 51 excited states used with an excitation energy cut-off of 25 eV.

Two isotopes of CH⁺ are considered in this paper: ¹²CH⁺ and ¹³CH⁺ the calculated equilibrium geometry dipole moment and rotational constant of ¹²CH⁺ and ¹³CH⁺ are the same to five significant figures and are $\mu = 1.6711$ D and $B = 14.454$ cm⁻¹, respectively. The best available experimental value for the ¹²CH⁺ dipole is $\mu = 1.683$ D (Cheng et al. 2007) which was used to calculate rotational excitation cross-sections for ¹²CH⁺ and ¹³CH⁺. The CDMS rotational constant for ¹²CH⁺ $B = 13.931$ cm⁻¹ (Müller et al. 2005) was used for both ¹²CH⁺ and ¹³CH⁺.

2.1.4 Cross-sections and rate coefficients

Each of the above calculations produces four fixed-nuclei **T**-matrices for each molecule (one for each irreducible representation in C_{2v} symmetry) for electron collision energy considered. These **T**-matrices are used to calculate the rotational excitation cross-sections for the molecules using program ROTIONS (Rabadán & Tennyson 1998). ROTIONS computes the rotational excitation cross-sections for each transition of the rotational angular momentum quantum number J . It is also useful to look at the cross-sections in terms of ΔJ , the change in the angular momentum quantum number.

$\Delta J = 1$ transitions are strongly influenced by the long-range effect of the dipole moment and ROTIONS employs the Coulomb-Born approximation to include the contributions of higher partial waves ($\ell > 4$) to the cross-sections. These long-range effects have been demonstrated to be unimportant for other transitions (Faure & Tennyson 2001). The best available value of the dipole moment was used in these calculations.

The adiabatic nuclear rotation (ANR) method was employed to calculate the cross-sections. The ANR approximation is valid when the electron collision time is less than the period of rotational motion. The suitability of the ANR method to diatomic, molecular ions is explained in Chang & Temkin (1970). As explained by Faure et al. (2006) the ANR method becomes invalid close to a rotational threshold because it neglects the rotational Hamiltonian. A kinetic-scaling method, scaling with a kinematic momentum ratio solves this problem for neutral molecules but not, however, for ions, see Faure et al. (2006) and references therein. This kinetic-scaling method has been employed in the previous **R**-matrix studies on HeH⁺ and CH⁺ and the cross-sections published in these studies can be said, therefore, to be erroneous in the vicinity of the rotational threshold. For this publication the threshold energy for rotational excitation cross-sections was calculated from the experimental rotational constant of the molecule and cross-sections below

this threshold were simply set to zero. This form of threshold ‘correction’ is in accord with the Wigner law and has been shown to be much more accurate (Faure et al. 2006) than the more complicated kinetic scaling employed in the previous **R**-matrix studies on HeH⁺ and CH⁺. Note that closed-channel effects are neglected but these are expected to be small for polar ions (Faure et al. 2006). This methodology was shown to work well in the only available experimental test of electron impact rotational (de-)excitation rates (Shafiret et al. 2009).

In practice, we have considered rotational transitions between levels with $J \leq 10$. Transitions were however restricted to $\Delta J \leq 8$ owing to the limited number of partial waves in the **T**-matrices ($\ell \leq 4$). Excitation cross-sections were computed for collision energies E_{coll} in the range 0.01–5 eV. For transitions with a rotational threshold below 0.01 eV, cross-sections were extrapolated down to the threshold using a $1/E_{\text{coll}}$ (Wigner’s) law, as recommended by Faure et al. (2006). Assuming that the electron velocity distribution is Maxwellian, rate coefficients for excitation transitions were obtained for temperatures in the range 1–3000 K. Going to higher temperatures would require the inclusion of $\Delta J \geq 8$ transitions for the results to converge. Furthermore the energy range 1–3000 K is considered complete for the ISM. De-excitation rate coefficients were obtained using the detailed balance relation.

3 RESULTS

The supplementary data associated with this paper includes rotational excitation and de-excitation rate coefficients for HeH⁺, the two isotopes of CH⁺: ¹²CH⁺ and ¹³CH⁺, and the three isotopes of ArH⁺: ³⁶ArH⁺, ³⁸ArH⁺ and ⁴⁰ArH⁺. The data sets are published for transition with starting values of $J = 0 - 11$ which is complete for the temperature range 0–3000 K with $\Delta J = 1 - 8$.

We start by considering results for electron-impact rotational excitation of HeH⁺ and ¹²CH⁺ (henceforth in this paper to be referred to simply as CH⁺) since there are previous studies on these systems against which we can compare.

3.1 HeH⁺

Fig. 1 shows our rate coefficients for rotational excitation of HeH⁺. As expected the $\Delta J = 1$ excitation is the dominant process, particularly at low temperatures. However, as observed by Rabadán et al. (1998), the $\Delta J = 2$ excitation rate approaches that of $\Delta J = 1$ for electron temperatures above 100 K, where it differs by only about a factor of two. This should make the HeH⁺ $J = 2 - 1$ emission line at 74.7848 μm (Matsushima, Oka & Takagi 1997) of similar strength to the $J = 1 - 0$ line at 149.137 μm . Although both these far-infrared lines lie at wavelengths which are difficult to study from the ground, the possibility of observing two lines should significantly enhance the prospect of observing this elusive but fundamental species.

Fig. 2 compares the rate coefficients for key electron-impact HeH⁺ excitation transitions with the previous results of Rabadán et al. (1998). The agreement is generally very good. This is not surprising since the electronic simplicity of the HeH⁺ system meant that the earlier study was already based on excellent electronic wavefunctions (Sarpal, Tennyson & Morgan 1991a) which had already been demonstrated by detailed comparisons with experiment for the HeH Rydberg molecule (Sarpal et al. 1991b). The largest differences between the previous study and our new results occur at low temperatures where our rate coefficients are increased. This is due to our improved treatment of threshold effects in the ANR

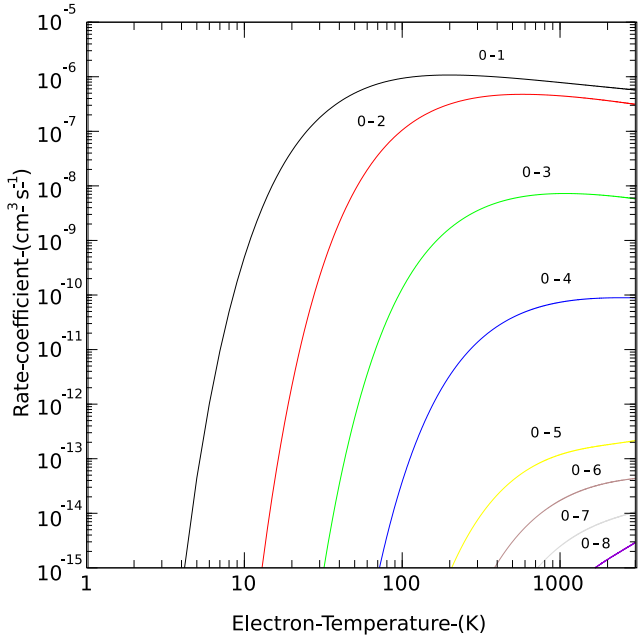


Figure 1. Rate coefficients for rotational excitation of HeH⁺ from the ground state ($J=0$) to the lowest eight excited states.

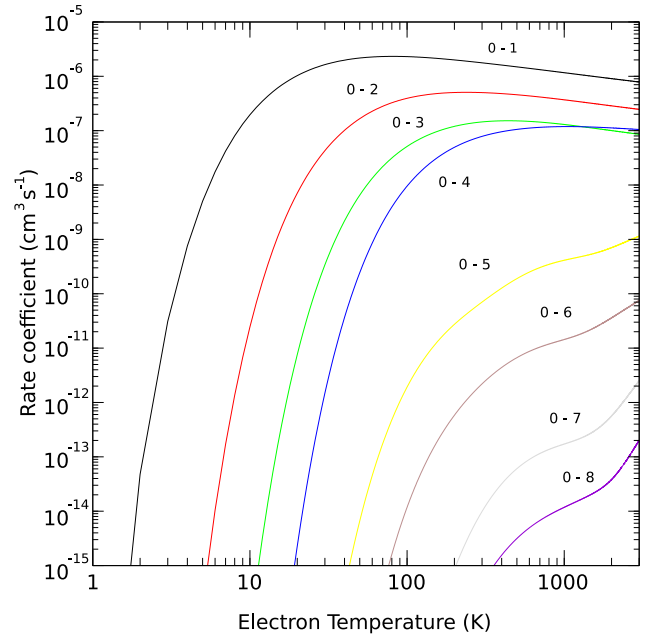


Figure 3. Rate coefficients for rotational excitation of CH⁺ from the ground ($J=0$) state to the lowest eight excited states.

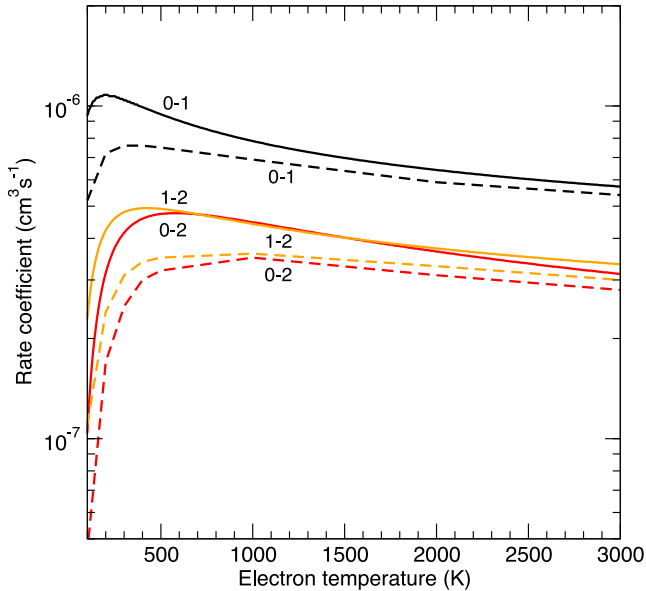


Figure 2. Rate coefficients for rotational excitation of HeH⁺ from Rabadán et al. (1998) (—) against our results (---).

approximation. For this reason we believe our new results to be more accurate.

3.2 CH⁺

The situation for CH⁺ is somewhat different in that our new results differ significantly from the previous predictions. Fig. 3 summarizes our results. As might be expected, given that CH⁺ has a large permanent dipole, we find that the excitation process is dominated by $\Delta J = 1$ transitions.

These rate coefficient can be compared with those calculated in a previous R-matrix study by Lim et al. (1999). These authors found

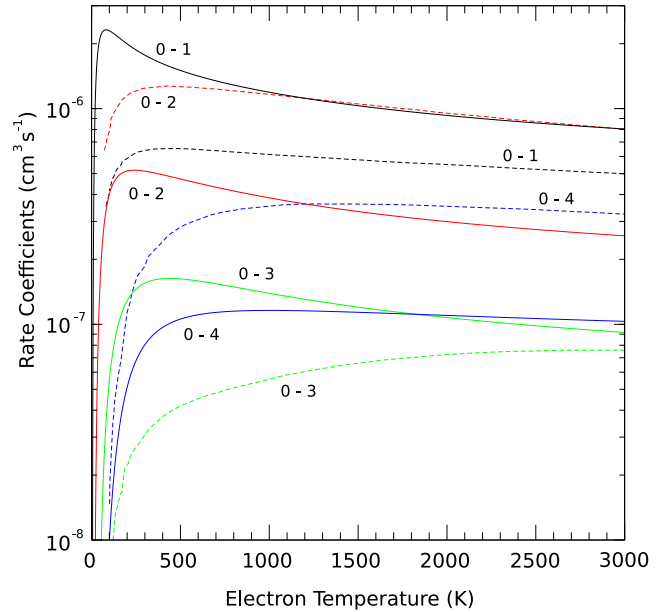


Figure 4. Rate coefficients for rotational excitation of CH⁺ from Lim et al. (1999) (---) against our results (—).

the rotational excitation cross-sections for the $\Delta J = 2$ transitions to be greater than $\Delta J = 1$ transitions. A comparison with these results is shown in Fig. 4. CH⁺ is a difficult system to construct accurate electron collision wavefunctions for, due to presence of low-lying electronically excited states (Tennyson 1988; Madden, Tennyson & Zhang 2011). We suggest that the previous study overestimates the role of $\Delta J = 2$ transitions for this strongly dipolar system and our new results should be adopted.

Our rotational excitation cross-sections for $\Delta J = 3$ and $\Delta J = 4$ transitions in CH⁺ agree quite well (within a factor of 2) with

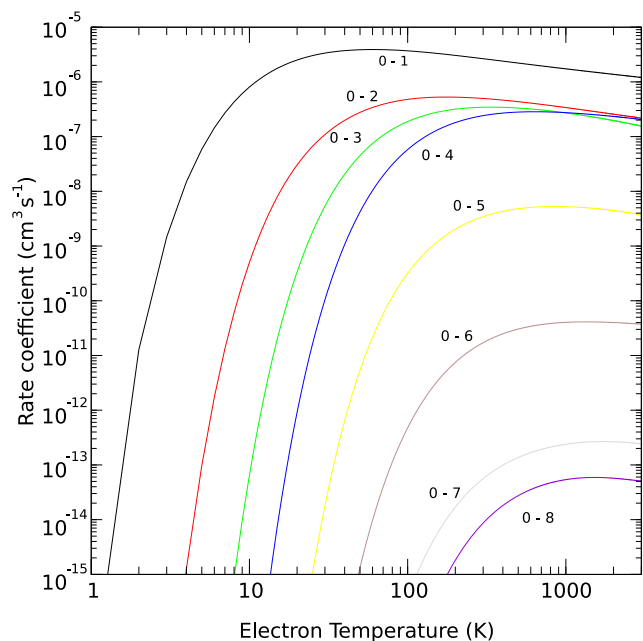


Figure 5. Rate coefficients for rotational excitation of $^{36}\text{ArH}^+$ from the ground state ($J = 0$) to the lowest eight excited states.

those of Lim et al. (1999) at high temperatures where the $\Delta J = 4$ cross-section is greater. The agreement is however less good at low temperatures where we find the $\Delta J = 3$ transition to be more important; this change is largely due to our improved treatment of threshold effects. Our new calculations also shows the $\Delta J = 6$ transition to be much lower than previously shown; this is again as expected.

3.3 ArH^+

Fig. 5 presents rate coefficients for electron-impact rotational excitation of $^{36}\text{ArH}^+$ from its rotational ground state. Figs 6 and 7 present rate coefficients for $^{38}\text{ArH}^+$ and $^{40}\text{ArH}^+$, respectively. As expected the processes are dominated by $\Delta J = 1$ transitions. Interestingly, above 100 K the rates for $\Delta J = 2$, $\Delta J = 3$ and $\Delta J = 4$ transitions become increasingly similar. Rates for higher excitations are all negligible.

4 ARH^+ EXCITATION IN THE CRAB NEBULA

The first detection of $^{36}\text{ArH}^+$ in space was reported by Barlow et al. (2013) using the *Herschel Space Observatory*. The $j = 1 - 0$ and $2 - 1$ rotational lines were identified in emission at several positions in the Crab nebula. This supernova remnant is known to contain filaments where enhanced emission of both H_2 and Ar^+ is observed. From the modelling of the two rotational lines, Barlow et al. (2013) concluded that the likely excitation mechanism is electron collisions in regions where the electron density n_e is a few $\times 100 \text{ cm}^{-3}$ and the temperature is about 3000 K. However, as collisional data were not available for ArH^+ , Barlow et al. (2013) employed the $\text{CH}^+ + e^-$ collisional rates of Lim et al. (1999) in place of those for $\text{ArH}^+ + e^-$. The $^{36}\text{ArH}^+$ column density was estimated as $10^{12} - 10^{13} \text{ cm}^{-2}$, with lower limits for the isotopic ratios $^{36}\text{ArH}^+ / ^{38}\text{ArH}^+ > 2$ and $^{36}\text{ArH}^+ / ^{40}\text{ArH}^+ > 4$. As can be seen from Figs 4 and 5, the $\text{CH}^+ + e^-$ collisional rates of Lim et al. (1999) differ significantly from those

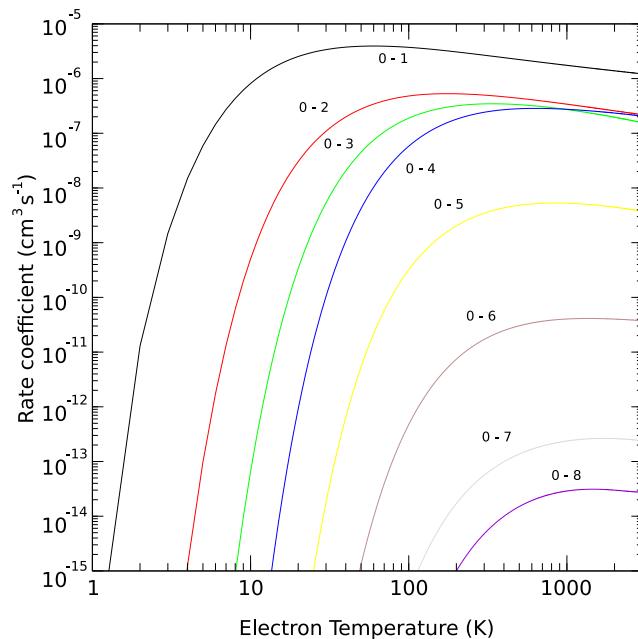


Figure 6. Rate coefficients for rotational excitation of $^{38}\text{ArH}^+$ from the ground state ($J = 0$) to the lowest eight excited states.

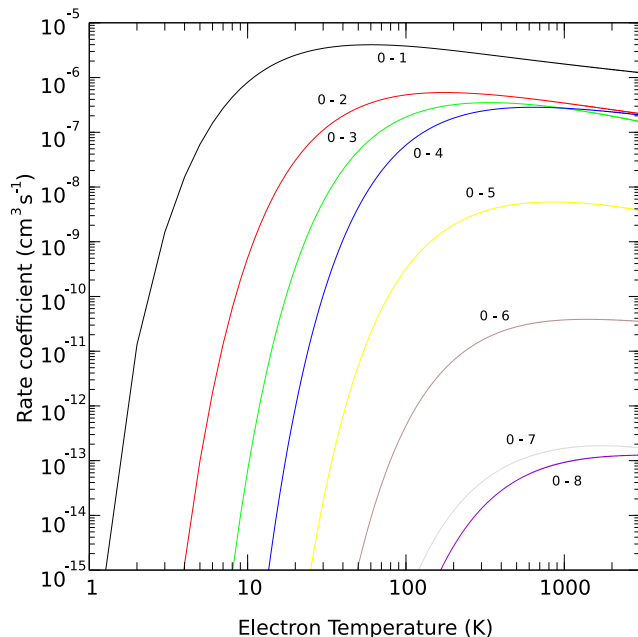


Figure 7. Rate coefficients for rotational excitation of $^{40}\text{ArH}^+$ from the ground state ($J = 0$) to the lowest eight excited states.

computed by us for $\text{ArH}^+ + e^-$, so that different excitation conditions and/or column densities are expected.

A new model for the excitation of ArH^+ in the Crab nebula is presented here using the above **R**-matrix electron-impact excitation rates and the radiative rates taken from the CDMS (Müller et al. 2005). Radiative transfer calculations were performed with the RADEX code (van der Tak et al. 2007), using the Large Velocity Gradient (LVG) approximation for an expanding sphere. The physical conditions in the molecular gas associated with the filaments and knots in the Crab nebula were measured by

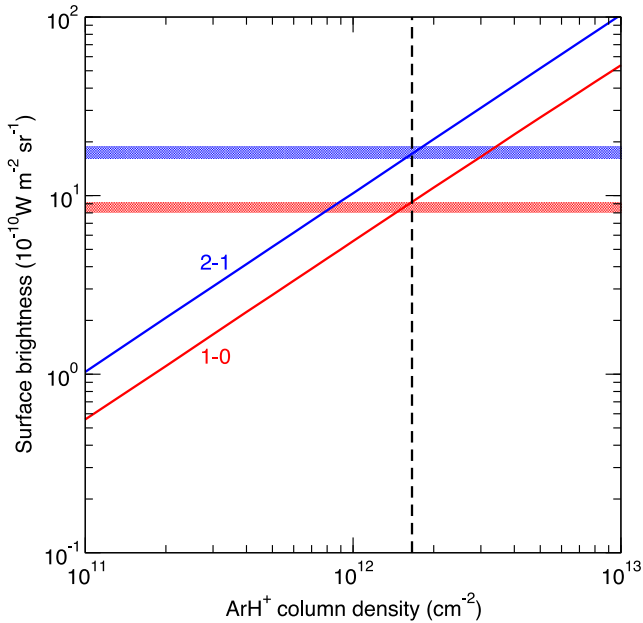


Figure 8. Surface brightness (in $10^{-10} \text{ W m}^{-2} \text{ sr}^{-1}$) for the $j = 1 - 0$ and $2 - 1$ rotational lines of $^{36}\text{ArH}^+$ from the Crab nebula as function of column density. The blue and red hatched zone show the observational results of Barlow et al. (2013) at the position of the SLW C4 and SSW B3 SPIRE detectors.

Loh et al. (2012). These authors employed emission lines from ortho- H_2 to derive (molecular) temperatures in the range ~ 2200 – 3200 K. In addition, emission lines from atomic S^+ were used to estimate $n_e \sim 1400$ – 2500 cm^{-3} , from which total hydrogen densities ($n_{\text{H}} = n(\text{H}^+) + n(\text{H}) + 2n(\text{H}_2)$) in the range $\sim 14\,000$ – $25\,000$ were inferred (Loh et al. 2012). As electron-impact rate coefficients for dipolar transitions are typically 10^4 – 10^5 larger than those of neutrals, collisions with H and H_2 can be safely neglected. Assuming that the proton (H^+) fraction is small in the filaments, electrons should be the dominant colliding species, with a fraction $n_e/n_{\text{H}} \sim 0.1$. The electron density and temperature were fixed in our calculations at $n_e = 2000 \text{ cm}^{-3}$ and $T = 3000$ K. The line width (FWHM) is unresolved with *Herschel*/SPIRE but it was taken here as 20 km s^{-1} , as expected in the molecular gas of the nebula (Richardson et al. 2013). Finally, the column density of $^{36}\text{ArH}^+$ was varied from 10^{11} to 10^{13} cm^{-2} .

Our results are presented in Fig. 8 for a position in the Crab nebula where both the $j = 1 - 0$ and $2 - 1$ lines were detected (SLW C4 and SSW B3 detectors, respectively, see Barlow et al. 2013). It is found that the observed surface brightnesses of the two rotational lines can be reproduced simultaneously by our model for a column density of $\sim 1.7 \times 10^{12} \text{ cm}^{-2}$. This value is in good agreement with the lower limit of Barlow et al. (2013), as expected from our higher electron density and larger $0 \rightarrow 1$ collisional rates. It should be noted that the surface brightnesses at other positions in the nebula are similar, within a factor of ~ 3 , suggesting similar column densities. We can also notice that the surface brightnesses increase linearly with the column density, as expected in the optically thin regime (opacities are much lower than unity).

In order to test the influence of the electron density, we show in Fig. 9 the sensitivity of the $(2 - 1)/(1 - 0)$ line emission ratio. The ratio derived by Barlow et al. (2013) at the above position in the nebula is ~ 2 and it was found to be very similar (~ 2.5) on a bright knot. In our LVG calculations the temperature is still

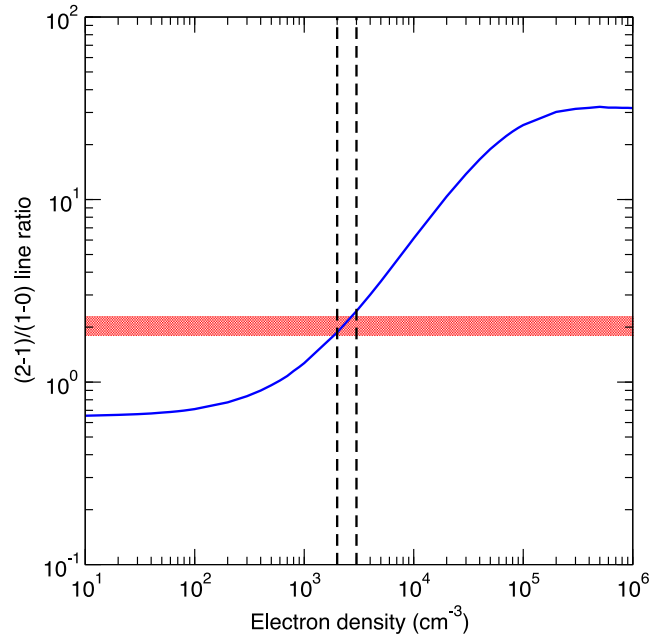


Figure 9. Plot of the $(2 - 1)/(1 - 0)$ line surface brightness ratio predicted for a $^{36}\text{ArH}^+$ column density of $2 \times 10^{12} \text{ cm}^{-2}$. The red hatched zone shows the observational result of Barlow et al. (2013) at the position of the SLW C4 and SSW B3 SPIRE detectors.

fixed at $T = 3000$ K and the column density at $N(\text{ArH}^+) = 2 \times 10^{12} \text{ cm}^{-2}$. On Fig. 9 it is observed that at high electron density ($n_e > 10^5 \text{ cm}^{-3}$), when the rotational populations are thermalized (i.e. at LTE), the line ratio is ~ 31 . The ratios observed in the Crab nebula therefore suggest a strongly non-LTE excitation of ArH^+ . We also observe that the line ratio strongly decreases with decreasing electron density. Our model thus requires electron densities in the range 2 – $3 \times 10^3 \text{ cm}^{-3}$ to reproduce the observed ratio, in very good agreement with the values derived by Loh et al. (2012) from S^+ lines. The line ratio was also found to depend only very weakly on column density (in the range 10^{11} to 10^{13} cm^{-2}) and temperature (in the range 2000 – 3000 K). As a result, the $(2 - 1)/(1 - 0)$ emission line ratio of ArH^+ is found to provide a robust and accurate measurement of the electron density in hot and highly ionized region of the molecular ISM.

5 CONCLUSIONS

In this paper, we present electron-impact rotational rate coefficients for diatomic hydride cations of great astrophysical interest. A complete set of data has been placed in the BASECOL (Dubernet et al. 2013) and LAMDA (Schöier et al. 2005) data bases. These data comprise electron-impact rotational excitation and de-excitation rate coefficients for HeH^+ , $^{12}\text{CH}^+$, $^{13}\text{CH}^+$, $^{36}\text{ArH}^+$, $^{38}\text{ArH}^+$ and $^{40}\text{ArH}^+$, for all transitions $\Delta J = 1 - 8$ involving initial states of $J = 0 - 10$ for excitation and $J = 11 - 1$ for de-excitation. These (de)excitation rates should provide useful inputs for models of a variety of different astronomical environments where molecular ions are formed. We have in particular employed the $^{36}\text{ArH}^+$ data to model the $1 - 0$ and $2 - 1$ emission lines observed by the *Herschel Space Observatory* towards the Crab nebula. These data have allowed us to derive both the $^{36}\text{ArH}^+$ column density and the electron density in this source. Finally we note that both $^{36}\text{ArH}^+$ and $^{38}\text{ArH}^+$ have recently been detected in an extragalactic source (Müller et al.

2015), the collisional data provided here should prove useful in interpreting such observations.

ACKNOWLEDGEMENTS

This work has been supported by an STFC CASE studentship, grant number ST/K004069, for JRH, the Agence Nationale de la Recherche (ANR-HYDRIDES), contract ANR-12-BS05-0011-01 and by the CNRS national programme ‘Physico-Chimie du Milieu Interstellaire’. Philippe Salomé is acknowledged for useful discussions on the Crab nebula.

REFERENCES

- Amitay Z., Zajfman D., 1996, *Phys. Rev. A*, 54, 4032
 Barlow M. J. et al., 2013, *Science*, 342, 1343
 Carr J. M. et al., 2012, *Euro. J. Phys. D*, 66, 58
 Chang E. S., Temkin A., 1970, *J. Phys. Soc. Japan*, 29, 172
 Cheng M., Brown J. M., Rosmus P., Linguerrri R., Komihana N., Myers E. G., 2007, *Phys. Rev. A*, 71, 012502
 De Luca M. et al., 2012, *ApJ*, 751, L37
 Douglas A. E., Herzberg G., 1941, *AJ*, 94, 381
 Dubernet M.-L. et al., 2013, *A&A*, 553, A50
 Faure A., Tennyson J., 2001, *MNRAS*, 325, 443
 Faure A., Kokoouline V., Greene C. H., Tennyson J., 2006, *J. Phys. B: At. Mol. Opt. Phys.*, 39, 4261
 Gerin M. et al., 2010, *A&A*, 521, L16
 Godard B. et al., 2012, *A&A*, 540, A87
 Gómez-Carrasco S. et al., 2014, *ApJ*, 794, 33
 Indriolo N., Neufeld D. A., Gerin M., Geballe T. R., Black J. H., Menten K. M., Goicoechea J. R., 2012, *ApJ*, 758, 83
 Indriolo N., Neufeld D. A., Seifahrt A., Richter M. J., 2013, *ApJ*, 764, 188
 Jimenez-Redondo M., Cueto M., Luis-Domenech J., Tanarro I., Herrero V., 2014, *RSC Adv.*, 4, 62030
 Lepp S., Stancil P. C., Dalgarno A., 2002, *J. Phys. B: At. Mol. Opt. Phys.*, 35, 57
 Lim A. J., Rabadán I., Tennyson J., 1999, *MNRAS*, 306, 473
 Liu X.-W. et al., 1997, *MNRAS*, 290, L71
 Loh E. D., Baldwin J. A., Ferland G. J., Curtis Z. K., Richardson C. T., Fabian A. C., Salomé P., 2012, *MNRAS*, 421, 789
 Madden D., Tennyson J., Zhang R., 2011, *J. Phys. Conf. Ser.*, 300, 012017
 Matsushima F., Oka T., Takagi K., 1997, *Phys. Rev. Lett.*, 78, 1664
 Menten K. M., Wyrowski F., Belloche A., Güsten R., Dedes L., Müller H. S. P., 2011, *A&A*, 525, A77
 Miller S., Tennyson J., Lepp S., Dalgarno A., 1992, *Nature*, 355, 420
 Moorhead J. M., Lowe R. P., Maillard J. P., Wehlau W. H., Bernath P. F., 1988, *ApJ*, 326, 899
 Müller H. S. P., Schlöder F., Stutzki J., Winnewisser G., 2005, *J. Mol. Struct.*, 742, 215
 Müller H. S. P. et al., 2015, *A&A*, 582, L4
 Pavanello M., Bubín S., Molski M., Adamowicz L., 2005, *J. Phys. Chem.*, 123, 104306
 Rabadán I., Tennyson J., 1998, *Comput. Phys. Commun.*, 114, 129
 Rabadán I., Sarpal B. K., Tennyson J., 1998, *MNRAS*, 299, 171
 Richardson C. T., Baldwin J. A., Ferland G. J., Loh E. D., Kuehn C. A., Fabian A. C., Salomé P., 2013, *MNRAS*, 430, 1257
 Roueff E., Lique F., 2013, *Chem. Rev.*, 113, 12, 8906
 Sarpal B. K., Tennyson J., Morgan L. A., 1991a, *J. Phys. B: At. Mol. Opt. Phys.*, 24, 1851
 Sarpal B. K., Branchett S. E., Tennyson J., Morgan L. A., 1991b, *J. Phys. B: At. Mol. Opt. Phys.*, 24, 3685
 Sarpal B. K., Tennyson J., Morgan L. A., 1994, *J. Phys. B: At. Mol. Opt. Phys.*, 27, 5943
 Schilke P. et al., 2014, *A&A*, 566, A29
 Schöier F. L., van der Tak F. F. S., van Dishoeck E. F., Black J. H., 2005, *A&A*, 432, 369
 Shafir D. et al., 2009, *Phys. Rev. Lett.*, 102, 223202
 Tennyson J., 1988, *J. Phys. B: At. Mol. Opt. Phys.*, 21, 805
 Tennyson J., 2010, *Phys. Rep.*, 491, 29
 Tennyson J., Brown D. B., Munro J. J., Rozum I., Varambhia H. N., Vinci N., 2007, *J. Phys. Conf. Ser.*, 86, 012001
 van der Tak F. F. S., Black J. H., Schöier F. L., Jansen D. J., van Dishoeck E. F., 2007, *A&A*, 468, 627
 van der Tak F. F. S., Ossenkopf V., Nagy Z., Faure A., Röllig M., Bergin E. A., 2012, *A&A*, 537, L10
 van der Tak F. F. S., Nagy Z., Ossenkopf V., Makai Z., Black J. H., Faure A., Gerin M., Bergin E. A., 2013, *A&A*, 560, A95
 Werner H. J., Knowles P. J., Lindh R., Manby F. R., Schütz M., 2010, *MOLPRO*, A Package of ab initio Programs, available at <http://www.molpro.net/>
 Wyrowski F., Menten K. M., Güsten R., Belloche A., 2010, *A&A*, 518, A26
 Zinchenko I., Dubrovich V., Henkel C., 2011, *MNRAS*, 415, L78

SUPPORTING INFORMATION

Additional Supporting Information may be found in the online version of this article:

supdat.zip

diffjt.pdf

(<http://www.mnras.oxfordjournals.org/lookup/suppl/doi:10.1093/mnras/stv2429/-/DC1>).

Please note: Oxford University Press is not responsible for the content or functionality of any supporting materials supplied by the authors. Any queries (other than missing material) should be directed to the corresponding author for the article.

This paper has been typeset from a $\text{\TeX}/\text{\LaTeX}$ file prepared by the author.